Title Page

Cell-Based and Biochemical Structure-Activity Analyses of Analogues of the Microtubule

Stabilizer Dictyostatin

Brianne S. Raccor, Andreas Vogt, Rachel P. Sikorski, Charitha Madiraju, Raghavan

Balachandran, Kia Montgomery, Youseung Shin, Yoshikazu Fukui, Won-Hyuk Jung, Dennis P.

Curran, and Billy W. Day*

MOL #42598

Running Title Page

a) Running Title: Analogues of (–)-Dictyostatin

b) Corresponding Author: Billy W. Day, Ph.D.

10017 Biomedical Science Tower 3

3501 Fifth Avenue

Pittsburgh, PA 15213

Telephone: (412) 648-9706

Fax: (412) 383-5298

Email: bday@pitt.edu

c) Number of text pages: 21

Number of tables: 2

Number of figures: 5

Number of references: 40

Number of words in abstract: 248

Number of words in introduction: 689

Number of words in discussion: 1387

d) CPM, counts per minute; DMSO, dimethylsulfoxide; FITC, fluorescein isothiocyanate; GFA, genetic function approximation; K_d, equilibrium dissociation constant; K_i, equilibrium inhibition constant; MDEC, minimum detectable effective concentration; MSG, monosodium glutamate; MT, microtubule; QSAR, quantitative structure-activity relationship; SAR, structure-activity relationship.

Abstract

Compounds that bind to microtubules (MTs) and alter their dynamics are highly sought

due to the clinical success of paclitaxel and docetaxel. The naturally occurring compound (–)-

dictyostatin binds to MTs, causes cell cycle arrest in G2/M at nanomolar concentrations, and

retains antiproliferative activity in paclitaxel-resistant cell lines, making dictyostatin an attractive

candidate for development as an antineoplastic agent. Here we examined a series of dictyostatin

analogues to probe biological and biochemical structure-activity relationships. We used a high-

content multiparameter fluorescence based cellular assay for MT morphology, chromatin

condensation, mitotic arrest and cellular toxicity to identify regions of dictyostatin that were

essential for biological activity. Four analogues, namely 6-*epi*-dictyostatin, 7-*epi*-dictyostatin,

16-normethyldictyostatin and 15Z,16-normethyldictyostatin, retained low nanomolar activity in

the cell-based assay and were chosen for analyses with isolated tubulin. All four compounds

were potent inducers of MT assembly. Equilibrium binding constant (K_i) determinations using

[^{14}C]epothilone B, which has a three-fold higher affinity for the taxoid binding site than

paclitaxel, indicated that 6-*epi*-dictyostatin and 7-*epi*-dictyostatin displaced [^{14}C]epothilone B

with K_i values of 480 nM and 930 nM, respectively. 16-Normethyldictyostatin and 15Z,16-

normethyldictyostatin had reduced affinity (K_i values of 4.55 and 4.47 µM, respectively),

consistent with previous reports showing that C16-normethyldictyostatin loses potency in

paclitaxel-resistant cell lines that have a Phe270 to Val mutation in the taxoid binding site of β-

tubulin. Finally, we developed a set of QSAR equations correlating structures with

antiproliferative activity. The equations accurately predicted biological activity and will help in

the design of future analogues.

Microtubules (MTs) are formed from the heterodimeric protein tubulin. Tubulin is composed of two 50 kDa subunits, α- and β-tubulin, which share significant sequence homology (Howard and Hyman, 2003). The importance of microtubules (MTs) for mitosis and the potential to interfere with the delicate dynamics of MTs has led to the search for and development of many tubulin- and MT-interacting compounds. MT perturbing agents can be roughly classified into two groups based upon the mechanism by which they disrupt normal microtubule function. These include agents that stabilize MT polymer formation and agents that destabilize MTs or inhibit MT polymer formation. The first discovered example of the former class is paclitaxel (Taxol®) (Schiff et al., 1979), which has been used successfully in the treatment of breast, lung and ovarian carcinomas (Jordan and Wilson, 2004).

Since the discovery of paclitaxel, many other MT stabilizers have been identified from various natural sources, including discodermolide (Gunasekera et al., 1990), dictyostatin (Pettit et al., 1994), the epothilones (Bollag et al., 1995), cyclostreptin (Sato et al., 2000), peloruside A (Hood et al., 2002) and laulimalide (Mooberry et al., 1999). Except for laulimalide and peruloside A (Pryor, 2002 et al.; Gaitanos et al., 2004), all of these agents share a common binding site on β-tubulin. Of these agents, dictyostatin and discodermolide have the greatest affinity for the taxoid binding site, followed by epothilone B (Madiraju et al., 2005). Additionally, all of these agents retain activity against paclitaxel-resistant cell lines (Kowalski et al., 1997; Edler et al., 2005).

The structure of dictyostatin remained unknown for a decade because of the scarcity of compound. Finally in 2004, its structure was elucidated from high field NMR and computational analyses (Paterson et al., 2004a), and independently verified by two full syntheses (Paterson et al., 2004b; Shin et al., 2004). The chemical structure of dictyostatin closely resembles that of

discodermolide, and 10 of the 11 stereocenters in dictyostatin are shared with discodermolide.

We previously showed dictyostatin to be as potent as discodermolide in terms of MT nucleation ability and competition with [³H]paclitaxel for binding to the taxoid site on MTs (Madiraju et al., 2005). Structure-activity relationship (SAR) studies to search for the minimum structural elements that contribute to cytotoxicity and retain affinity for the taxoid site were applied here to dictyostatin analogues. A few analogues of dictyostatin and their relative potencies against several cancer cell lines have been reported by others (Paterson et al., 2007a; Paterson and Gardner, 2007b). We have synthesized several analogues in attempts to study the SAR of the dictyostatin scaffold (Fukui et al., 2006; Jung et al., 2007; Shin et al., 2007). From this collection of existing dictyostatin analogues, we chose several of them based on the structural differences between dictyostatin and discodermolide for detailed biological SAR studies (Figure 1). The C1-C9 chain is one of the main structural differences between the two natural products, and analogues designed for this purpose were epimers at C6, C7 and C9, and C2:C3 geometric isomers. From discodermolide SAR studies, it is has been established that removal of the C14 methyl group does not decrease cytotoxicity in the cancer cell lines tested. However, when C14-normethyldiscodermolide was tested in paclitaxel-resistant cell lines, cytotoxicity was greatly diminished, with IC_{50} values in the micromolar range (Smith et al., 2005). Since discodermolide can be considered an open chain form of the macrolactone of dictyostatin, a 16-*epi* open chain methyl ester analogue of the latter was included in our analysis. Finally, we made dictyostatin analogues containing a C15-C16 *Z*-alkene based on the fact that discodermolide possesses a C13-C14 *Z*-alkene, which is missing in dictyostatin, and two 20-member macrolactone *iso* analogues (Shin et al., 2005, Fukui et al., 2006; Jung et al., 2007; Shin et al., 2007).

To examine in detail the effects of these targeted structural modifications on biological

activity and the interaction with the proposed target, we used quantitative multiparameter

immunofluorescence assays to measure mitotic arrest and nuclear morphology in conjunction with

in vitro tubulin assembly and displacement studies using the potent taxoid site binding agent

epothilone B. Quantitative structure-activity relationship (QSAR) analyses were then employed to

correlate the structures with cytotoxic effects.

Materials and Methods

Materials. Dictyostatin was synthesized as described previously (Shin et al., 2004). The syntheses
of the analogues are reported elsewhere (Shin et al., 2005; Fukui et al., 2006; Jung et al., 2007;
Shin et al., 2007). Tubulin was isolated to electrophoretic homogeneity from fresh bovine brain
(Hamel and Lin, 1984). Paclitaxel was obtained from the Drug Synthesis and Chemistry Branch,
National Cancer Institute. Discodermolide, epothilone B and [^{14}C]epothilone B (specific activity
111 mCi/mmol) were generous gifts from Novartis Pharma AG. Rabbit anti-phosphohistone H3
antibody was purchased from Upstate Cell Signaling (Charlottesville, VA). Cy3-labeled donkey
anti-rabbit and FITC-labeled anti-mouse secondary antibodies were from Jackson Immunoresearch
(West Grove, PA). Guanosine 5'-triphosphate (GTP) and 2',3'-dideoxyguanosine-5'-triphosphate
(ddGTP) were purchased from USB (Cleveland, OH). All other chemicals including mouse anti-
alpha-tubulin antibody were purchased from Sigma (St. Louis, MO).

Methods.

High-content analysis of mitotic arrest. Detailed conditions for the high-content
analysis of microtubule stabilizers using a cell based immunofluorescence assay have been
described previously (Minguez, 2003). Briefly, HeLa cells were plated at a cell density of 8000
cells per well in collagen-1 coated 384-well microplates. Cells were allowed to attach and
spread for 3-8 h and treated with either vehicle (DMSO) or ten two-fold concentration gradients
of test agents and incubated for an additional 20 h at 37 °C. After the incubation, cells were
fixed with formaldehyde containing 10 µg/mL Hoechst 33342 to stain nuclei/chromatin,
permeabilized with Triton X-100 and simultaneously immunostained with antibodies against α-
tubulin (mouse monoclonal, Sigma cat. #T9026; 1:2500 dilution) and phosphohistone H3 (rabbit

polyclonal, Upstate cat. #06-50; 1:1000 dilution) followed by fluorescein-5-isothiocyanate

(FITC)-labeled donkey anti-mouse IgG (1:250) and Cy3-labeled donkey anti-rabbit IgG (1:250;

both from Jackson Immunoresearch). Each well was imaged on an ArrayScanII (Cellomics Inc.,

Pittsburgh, PA) using an Omega XF93 filter set at excitation/emission wavelengths of 350/461

nm (Hoechst), 494/519 nm (FITC) and 556/573 nm (Cy3). Images were analyzed with the

Target Activation Bioapplication (Cellomics, Inc.). The algorithm provided quantitative

measurements of nuclear FITC and Cy3 intensity, cell density, and mean and total nuclear

Hoechst 33342 intensities. Microtubule mass was defined as the average FITC intensity in an

area defined by the Hoechst-stained nuclei. To estimate the percentage of cells with elevated

phosphohistone H3 levels and with condensed chromatin, thresholds were defined as the average

intensity plus one standard deviation of Hoechst or Cy3 intensities in anti-phosphohistone H3- or

Hoechst 33342-stained cells, respectively, using a minimum of 1000 vehicle-treated cells per

well. Cells were classified as positive if their average intensities in the Hoechst or Cy3 channel

exceeded these thresholds. Cell density was defined as the number of nuclei per imaging field.

The EC_{50} was the effective concentration of drug that decreased cell density by 50% compared to

vehicle-treated control.

Tubulin assembly *in vitro*. Tubulin assembly was monitored by turbidity development

at 350 nm as described previously (Madiraju et al., 2005). Reaction mixtures (0.25 mL final

volume) contained tubulin (1 mg/mL; 10 μM), monosodium glutamate (MSG) (0.8 M from a

stock solution adjusted to pH 6.6 with HCl), DMSO (final volume 4% *v/v*) and test agent (10

μM). Reaction mixtures without test agent were cooled to 0 °C and added to quartz cuvettes held

at 0.25–0.5 °C a temperature-controlled (via a Peltier unit), 6-sample Beckman DU 7400

spectrophotometer (Beckman Coulter, Fullerton, CA). Test agent in DMSO was then rapidly

mixed into the reaction mixture. Absorbance at 350 nm was monitored in each cuvette every 15

sec. Each 6-sample run contained one positive control (paclitaxel, 10 µM final concentration)

and one negative control (DMSO only). Baselines were established at 0.25–2.5 °C. The

temperature was rapidly raised to 30 °C (in approximately 1 min) and held there for 20 min. The

temperature was then rapidly lowered back to 0.25–2.5 °C. The change in absorbance 20 min

after samples reached 30 °C was used to calculate the extent of polymerization. The change in

absorbance at 21 min in the paclitaxel sample was assigned as 100% assembly (positive control),

while the change in absorbance in the DMSO only sample (negative control) was assigned as 0%

assembly.

Radioligand displacement studies. Determination of the equilibrium binding constant

(K_d) for epothilone B was determined using methods described previously (Madiraju et al.,

2005). An 80 µM stock solution of [^{14}C]epothilone B was prepared in 50% DMSO. Samples of

[^{14}C]epothilone B at 0.005-2 µM were prepared in 4:1 (*v/v*) 0.75 M MSG/DMSO (total volume

50 µL) and warmed to 37 °C. Microtubules were preformed in separate tubes by incubating 2.5

µM tubulin and 25 µM ddGTP in 0.75 M MSG/DMSO for 30 min at 37 °C. Equal volumes (50

µL each) of the radiolabeled compound mixtures and microtubule solutions were mixed and

incubated for 30 min at 37 °C. Reaction mixtures were then centrifuged in a Beckman Allegra

TM 64R (Beckman-Coulter, Fullerton, CA) at 14,000 rpm for 30 min at room temperature. The

amount of radiolabel in the supernatant was determined by scintillation spectrometry in a

LS6500 Beckman multi-propose scintillation counter (Beckman-Coulter, Fullerton, CA). Non-

specific radiolabel binding was determined from competition experiments with 8 µM

discodermolide and processing as described above.

Inhibitors in 4:1 (v/v) 0.75 M MSG/DMSO were pre-incubated with radiolabeled compound in a final volume of 50 µL for 10 min at 37 °C. To this mixture, 50 µL of microtubules that were formed as described above were added, and the resulting mixture was incubated for 30 min at 37 °C. Reaction mixtures were centrifuged as described above, and a 50 µL aliquot of supernatant was analyzed by scintillation spectrometry.

Saturation binding data for $[^{14}C]$epothilone B were analyzed using a modified version of Swillens' equation that accounts for ligand depletion (Motulsky, 2003; Swillens, 1995):

$$\text{Total Binding} = \{((B_{max} \times ([L]_T - [L]_B))/(K_D + (([L]_T - [L]_B))\} + ([L]_T - [L]_B) \times NS \qquad \text{(Eq. 1)}$$

where B_{max} is the number of binding sites, $[L]_T$ is the amount of radioligand added, $[L]_B$ is the amount of ligand bound to tubulin polymer, and NS is the fraction of radioligand bound to nonspecific sites. Non-linear regression analysis was performed using GraphPad Prism software that allows for the simultaneous fitting of nonspecific and total binding data.

The equilibrium inhibition constant (K_i) values for dictyostatin and its analogues were determined using a modified Hanes analysis (Edler et al., 2005):

$$[S]/v = K_d \times (1 + [I]/K_i) + [S] \qquad \text{(Eq. 2)}$$

where [S] is the free concentration of $[^{14}C]$epothilone B, and v is the fractional saturation of microtubule sites by epothilone B and inhibitor. GraphPad Prism was used for linear regression, providing the $-K_d$ value as the x-intercept in the absence of inhibitor. The x-intercept in the presence of inhibitor, $-K_d(1+[I]/K_i)$, was used to calculate the K_i values.

QSAR. Molecular modeling and QSAR analyses were performed with the Cerius[2] suite

of programs (v. 4.5, Accelrys, Inc., San Diego, CA) utilizing the Merck Molecular Force

Field/CHARMM, the adopted-basis Newton-Raphson approach to molecular mechanics

minimizations in a dielectric field = 1, rigid body superimpositions based on atom similarities,

the MOPAC93 suite of semi-empirical molecular orbital algorithms and the genetic function

approximation as previously described (Verdier-Pinard et al., 1998).

Results

Cellular Effects of Dictyostatin and Its Analogues Determined By Multiparameter

Immunofluorescence Microscopy

We have reported previously the use of multiparameter high content analyses, a tool to acquire,

manage and retrieve information from multiparametric experiments to yield information about

the activity and spatial regulation of multiple targets in individual cells (Giuliano et al., 1997), to

characterize the responses of tumor cells to MT stabilizing agents (Minguez, 2003 et al.;

Madiraju et al., 2005). This assay provides information on the effects of such agents on MT

mass, histone H3 phosphorylation, nuclear morphology and cytotoxicity. HeLa cells were grown

in 384-well microtiter plates and treated with each compound for 21 h. The cells were fixed,

their nuclei stained with Hoechst 33342, permeabilized, MTs and phosphohistone H3 were

immunostained, and FITC- and Cy3-conjugated secondary antibodies were added. From Hoechst

staining, a nuclear mask was generated defining the area used to determine MT mass and

percentage of histone H3 phosphorylation. MT mass was determined from the cells' average

nuclear FITC intensity. Histone H3 phoshorylation was determined from the number of cells

with a higher pixel intensity for Cy3 than the average plus one standard deviation seen within

vehicle treated cells. Using a range of concentration of test agents, the minimum detectable

effective concentration (MDEC) was determined. The MDEC value is the minimum

concentration at which each agent causes a response in excess of vehicle-treated control cells

(Minguez et al., 2003). The MDECs for nuclear condensation, histone H3 phosphorylation, and

changes in MT morphology for dictyostatin and its analogues are shown in Table 1. For toxicity

determinations, cell densities were measured as Hoechst 33342 stained nuclei per imaging field.

The toxicity measurements in HeLa cells were consistent with those reported for other human

cancer cell lines, where the toxicity measure used was a decrease in absorbance at 490 nm after

cells treated with drug were exposed to 3-(4,5-dimethylthiazol-2-yl)-5-(3-

carboxymethoxyphenyl)-2-(4-sulfophenyl)-2*H*-tetrazolium (the MTS reagent) and *N*-

methylphenazine methylsulfate (Jung, 2007 et al.; Shin et al., 2007). Toxicity measurements and

the MDEC values generated from this initial screen provided a rapid and economical assessment

of the analogues' biological activities. As shown in Table 1, the 20-membered ring *iso* analogues

of dictyostatin, 16-*epi*-isodictyostatin and 15Z,16-normethylisodictyostatin, and 16-*epi*-

dictyostatin were inactive, yielding MDEC and EC_{50} values >5 μM. This led to the conclusions

that the 22-membered ring of dictyostatin is essential for retention of biological activity and that

if the C16 methyl group is present, it must be in the *S* configuration (Jung et al., 2007).

2*E*,15Z,16-Normethyldictyostatin analogue was considerably less active than 15Z,16-

normethyldictyostatin, proving that C2:3Z geometry is necessary for activity. From these data,

the four most potent analogues were chosen for further evaluation, namely 6-*epi*-dictyostatin, 7-

epi-dictyostatin, 16-normethyldictyostatin and 15Z,16-normethyldictyostatin.

　　　　Figure 2 illustrates the cellular phenotype observed after treatment with the four test

agents. MTs in cells treated with vehicle (panel A) were well organized, and the few cells

undergoing mitosis showed normal spindle formation. Cells treated with dictyostatin (panel B)

showed MT bundling and abnormal spindle formation, characteristic of cells treated with an MT

stabilizer. Panels C-F represent the images obtained when HeLa cells were treated with the

indicated concentrations of 6-*epi*-dictyostatin, 7-*epi*-dictyostatin, 15Z,16-normethyldictyostatin

or 16-normethyldictyostatin, respectively. All compounds produced morphological changes in

the cells similar to that of dictyostatin, including MT bundling and abnormal spindles.

Quantitative analysis showed that all compounds increased mitotic indices, nuclear condensation,

13

MT mass and a loss of cell density at nanomolar concentrations. 6-*epi*-Dictyostatin and 7-*epi*-dictyostatin affected all parameters at concentrations comparable to dictyostatin, whereas the 16-normethyl derivatives appeared to have lost some activity. Surprisingly, 15Z,16-normethyldictyostatin was more potent in all aspects than 16-normethyldictyostatin, which was the least potent agent. Thus, high-content analysis provided a rapid and efficient means to generate cellular SAR data on mitotic arrest, microtubule morphology and cytotoxicity. It demonstrated that the structural modifications made in the 6, 7, 15 and 16 positions did not significantly reduce compound activity in cells.

Determination of the Ability of Dictyostatin and Its Analogues to Induce Tubulin Assembly and Form Cold Stable Polymer

We previously reported that 16-normethyldictyostatin retains the ability to induce tubulin polymerization in the absence of GTP (Jung et al., 2007). To assess the hypernucleating ability of the dictyostatin epimers and olefin, we performed *in vitro* tubulin assembly assays under conditions in which polymerization does not occur in the absence of test agents and compared the analogues' activities to that of paclitaxel. Isolated tubulin was cooled to 2.5 °C, and test agents were added to a final concentration of 10 µM. The test agent-containing tubulin solutions were rapidly warmed to 30 °C to induce assembly, and after 20 min at 30 °C, the temperature was lowered to 0°C to test the cold stability of the polymer induced by the agents. Figure 3 shows that three agents were more active than the positive control (paclitaxel). Dictyostatin was the most potent compound in terms of nucleating and polymerizing ability, closely followed by 7-*epi*-dictyostatin and 6-*epi*-dictyostatin. There were some slight differences between the C6- and C7-epimers. 7-*epi*-Dictyostatin induced polymer formation more rapidly than did 6-*epi*-

14

dictyostatin, but the extent of polymerization caused by 6-*epi*-dictyostatin was greater. The

polymer formed with 6-*epi*-dictyostatin appeared more stable against cold-induced

depolymerization than the polymer from 7-*epi*-dictyostatin or dictyostatin itself. The nucleating

and polymerizing activities of 15Z,16-normethyldictyostatin and 16-normethyldictyostatin were

reduced but still comparable to those of paclitaxel.   Polymer induced by these two compounds

was cold stable.

Characterization of [^{14}C]Epothilone B Saturation Binding to Microtubules

We previously showed that dictyostatin and the four analogues have the ability to

compete with radiolabeled paclitaxel for binding to preformed MTs *in vitro* (Madiraju et al.,

2005; Jung et al., 2007). Here, we expanded on these preliminary observations by performing

detailed binding kinetics using [^{14}C]epothilone B. Epothilone B has an even higher affinity to

the taxoid site on tubulin than paclitaxel (Kowalski et al., 1997b). Because the saturation

binding kinetics of [^{14}C]epothilone B have not been reported, we first determined its K_d value for

the binding to MTs. The upper panel of Figure 4 shows the extent of non-specific binding of

[^{14}C]epothilone B bound to MTs in the presence and absence of 8 μM discodermolide. Fitting

the data using Swillens' modified equation (Eq. 1), which simultaneously fits total binding and

nonspecific binding, and accounts for ligand depletion, yielded a K_d value for epothilone B of

36.04 $\pm$ 1.58 nM. As the K_d value of paclitaxel is reported to be between 0.06-0.1 μM and since

the relative affinities of agents for the taxoid site followed the order paclitaxel < epothilone B <

discodermolide, the K_d value obtained in these experiments for epothilone B was considered

reasonable and acceptable (Buey et al., 2004).

Determination of Inhibition Constants for Dictyostatin and Its Analogues Utilizing

[^{14}C]Epothilone B in Competition Experiments

To determine the K_i values for dictyostatin and its analogues, a modified Hanes analysis

method (Eq. 2) was employed (Edler et al., 2005). The method uses the free concentration of

radioligand instead of the total concentration and also accounts for the free inhibitor

concentrations. As shown in the lower panel of Figure 4, plots of free concentration of

[^{14}C]epothilone B versus free substrate (*S*) divided by the fractional saturation (ν; used instead of

enzyme velocity) for 6-*epi*-dictyostatin yielded plots of parallel lines with slopes close to 1. The

K_d value for [^{14}C]epothilone B, determined from the negative intercept on the x-axis, was $50 \pm$

20 nM, close to the value obtained from the saturation experiments in the upper panel of Figure

4. As shown in Table 2, 16-normethyldictyostatin and 15Z,16-normethyldictyostatin gave the

highest K_i values, reflecting their reduced binding affinity. The K_i value for 15Z,16-

normethyldictyostatin was 4.47 ± 0.28 μM and the value for 16-normethyldictyostatin was 4.55

± 0.41 μM. These data correlated with the tubulin polymerization data, which showed that 16-

normethyldictyostatin and 15Z,16-normethyldictyostatin were the least potent of the compounds

in nucleation and MT stabilization experiments (Figure 3). Dictyostatin showed the highest

affinity for the taxoid site, with a K_i value of 70 ± 20 nM. Based on their effects on MT

assembly, it was surprising to find that 6-*epi*-dictyostatin and 7-*epi*-dictyostatin had substantially

less affinity under the conditions of the competition experiments, yielding K_i values of 480 ± 70

nM and 930 ± 310 nM, respectively.

QSAR Analyses

16

Using the NMR-derived solution structure of discodermolide as a template (Smith, 2001),
molecular models of dictyostatin, its analogues, discodermolide and 14-
normethyldiscodermolide were built. The lowest energy conformers of the models were found by
exhaustive molecular mechanics minimization, and then all models were superimposed onto that
of discodermolide. The only structures that did not superimpose well were 2E,15Z,16-
normethyldictyostatin and the 20-member *iso* analogues.   A large number of thermodynamic,
electronic, steric and linear free energy descriptors were then calculated for each model.

At this point we needed to decide upon the biological metric to use for the "activity" portion
of the QSAR. We chose the 50% growth inhibitory concentrations (GI$_{50}$) of the compounds
against human ovarian carcinoma 1A9 cells, which express wild type β-tubulins. Because the
number of descriptors far exceeded the number of compounds studied, the genetic function
approximation (GFA) was used to fit the data to the smallest possible number of descriptors. In
the GFA approach, a random population of equations is generated, their fitness is determined by
a number of statistical metrics (in particular Friedman's lack of fit score and R^2), and then the
equations are "evolved" by inclusion of combinations (child) from two of the best equations
(parents) (Verdier-Pinard et al., 1998). This process is reiterated (each iteration is termed a
"generation"), with a given frequency of "mutation" (random descriptor loss or use) incorporated
into each iteration until the best descriptors and QSAR equations are found. The five best
(according to statistical metrics) equations from 100,000 generations were:

–(logGI$_{50}$) = –0.017328 – 0.41287(rotable bonds) + 0.091723 (HF_MOPAC) –

0.223325(HF) + 0.0611096(dipole_MAG)   (Eq. 3)

$$-(logGI_{50}) = -26.5019 + 0.03692(area) - 0.328785(rotable\ bonds) - 0.04374(HF) +$$

$$0.924229(dipole\_MOPAC) \hspace{4cm} \text{(Eq. 4)}$$

$$-(log\ GI_{50}) = -26.3842 + 0.1088(area) + 1.31599\ (dipole\_MOPAC) - 0.353032(MR) +$$

$$0.654779(logP) \hspace{5cm} \text{(Eq. 5)}$$

$$-(logGI_{50}) = 1.694349 - 0.305704(rotable\ bonds) - 0.135425(HF) +$$

$$0.605182(dipole\_MOPAC) - 0.053736(HF\_MOPAC) \hspace{2cm} \text{(Eq. 6)}$$

$$-(logGI_{50}) = -48.6935 - 0.200571(MR) - 0.270041(rotable\ bonds) +$$

$$1.27617(dipole\_MOPAC) + 0.117247(area) \hspace{3cm} \text{(Eq. 7)}$$

where *rotable bonds* is the number of single bonds contained within the molecule, *HF* is the heat

of formation (the change in enthalpy for forming a molecule from its constituent atoms)

calculated with PM3 in MOPAC, *logP* is the calculated octanol-water partition coefficient, *MR* is

molar refractivity, *area* describes the Van der Waals area of a molecule, and the *dipole* terms are

the indicated vector within or a sum of all the vectors describing the dipole moment of the

molecule.

To determine the most significant descriptors in each equation, a "leave one (descriptor)

out" exercise was performed. This entailed calculating the activity with one of the descriptors

set to zero and then the deviation of the resulting value from the predicted activity when all

descriptors were used. For equations 4, 5 and 7, the most important contributors to activity were

18

area and molar refractivity. For equations 3 and 6, the most important descriptor was the heat of formation.

The predicted activity values generated from these equations were plotted versus the actual activity in the 1A9 cells to determine correlations. As shown in Figure 5, plotting of the –log molar predicted values generated from equation 3 versus the –log molar actual values led to an R^2 of 0.943. Values for R^2 of the other four equations were also > 0.93.

Discussion

A multiparameter fluorescence based cellular assay was used as an initial screen of dictyostatin and its analogues. Several conclusions were reached about the SAR for dictyostatin based on the compounds' effects on HeLa cell proliferation, histone H3 phosphorylation, MT mass and nuclear morphology. The importance of a 22-membered ring was proven by the inactivity of the 20-membered analogues 16-*epi*-isodictyostatin and 15Z,16-normethylisodictyostatin. If the C16 methyl group is present it must be in the *S* configuration, which is seen by the complete loss in activity of the 16-*epi*-dictyostatin analogue. C2:3Z geometry is also necessary. The most potent analogues from this initial screen were 6-*epi*-dictyostatin, 7-*epi*-dictyostatin, 16-normethydictyostatin and 15Z,16-normethyldictyostatin. Only minor differences in these four compounds' cellular activities were observed, although 6-*epi*-dictyostatin and the parent compound were the most active agents in all experiments. This is consistent with data from antiproliferative assays with 1A9 human ovarian cancer cells, where all of these analogs were shown to be potent inhibitors of cell proliferation with IC_{50} values in the low nanomolar range (Jung et al., 2007).

Although, qualitatively, the rank order of cellular activities correlated with the *in vitro* activities, there were some differences in the compounds' abilities to cause *in vitro* tubulin assembly and in the binding site affinity studies. Notably, the 16-normethyl derivatives 15Z,16-normethyldictyostatin and 16-normethyldictyostatin had almost 5-fold higher K_i values as compared to the C6- and C7-epimers. This is consistent with the hypothesis that the C16 methyl group is important in binding to the taxoid site through a key interaction with Phe270 on β-tubulin. Our recent report shows that 16-normethyldictyostatin has decreased potency in the paclitaxel-resistant 1A9/PTX10 ovarian cancer cell line, which has a Phe270 to Val point mutation in the taxoid binding site (Giannakakou et al., 1997; Shin, 2005). This is in agreement with our present results, where the lower affinity observed in competition experiments with 15Z,16-normethyldictyostatin and 16-normethyldictyostatin can be attributed to the loss of the favorable interaction of the C16 methyl group of dictyostatin with Phe270 in β-tubulin.

As observed from a similar loss in potency in the 1A9/PTX10 line, the interaction between the benzoyloxy group of paclitaxel and Phe270 of β-tubulin is important for paclitaxel's activity (Giannakakou et al., 1997). The importance of the interaction between Phe270 and methyl substituents in dictyostatin, epothilone B, and discodermolide is now becoming well established. Molecular modeling studies have suggested that the C14 methyl group of discodermolide is positioned in a favorable interaction with Phe270 in the hydrophobic binding pocket of the taxoid site (Xia et al., 2006). The importance of this interaction has been confirmed by the decrease of nucleating ability of 14-normethyldiscodermolide in tubulin polymerization assays (Smith et al., 2005). A 2D NMR-derived binding model of epothilone A to the tubulin heterodimer suggests the increased potency of epothilone B over epothilone A is due to the interaction of the C12 methyl with Phe270 (Reese et al., 2007).

As shown by our QSAR studies, the size of the molecule (area and molar refractivity) is the most significant contributor to cytostatic activity against 1A9 ovarian cancer cells. A loss of a methyl substituent would certainly lead to a decrease in the van der Waals surface area of the molecule and, according to our calculations, leads to a decrease in activity. Molar refractivity is a measure of the volume occupied by the molecule.   It is dependent on a number of factors such as molecular weight, refractive index, and density. This descriptor relates to the London dispersive forces that act in the drug-receptor interactions (Padron et al., 2002). Again, 16-normethyldictyostatin, and 15Z,16-normethyldictyostatin would be expected to have molar refractivities differing from those of dictyostatin and its C6 epimer, whose molar refractivities are identical.

Changes to the C6 and C7 stereocenters of dictyostatin were explored because they are present in the structure of discodermolide as its C4 and C5 carbons, part of its delta lactone ring. The multiparameter immunofluorescence studies with 6-*epi*-dictyostatin and 7-*epi*-dictyostatin showed that these analogues produced MT bundling and abnormal spindle formation at nanomolar concentrations. Their ability to produce these various cellular responses was observed at lower concentrations than required with dictyostatin. Although there was a slight loss in nucleation ability in tubulin polymerization assays, these compounds retained their ability to induce assembly of microtubules and to form cold stable polymer. Also, both compounds still had a high affinity for the taxoid site on β-tubulin, with the K_i values determined in competition experiments with [^{14}C]epothilone B of 480 nM and 930 nM for 6-*epi*-dictyostatin and 7-*epi*-dictyostatin, respectively. From these experiments it can be said that single stereochemical changes to this area are not only well tolerated, but lead to no loss in potency *in vivo*.

21

The saturation binding kinetics of epothilone B were characterized. One of the

fundamental assumptions of equilibrium binding is that only a small amount of substrate binds to

its target, leaving the relative amount of free substrate concentration unchanged. Ligand

depletion occurs if more than 10% of the substrate binds to the protein (Motulsky and

Christopoulous, 2003). When ligand depletion occurs, this assumption is invalidated and can, if

not taken into account, cause errors in data analysis (Morton et al., 2002; Carter et al., 2007).

This problem is commonly encountered in the centrifuge-based assay used to determine the

kinetics of MT stabilizing agents. For this reason, the saturation binding data was analyzed

using the modified Swillens' equation (Eq. 1), which not only accounts for ligand depletion but

also fits total binding and non-specific binding simultaneously. Fitting the non-specific and total

binding data simultaneously allows for the calculation of free ligand, and defines non-specific

binding as a constant fraction of the free ligand concentration. The K_d value obtained using this

analysis was reasonable as a measure of the affinity of epothilone B for the taxoid site in

comparison to results from previous competitive inhibition studies Kowalski et al., 1997;

Madiraju et al., 2005).

The binding kinetics of dictyostatin and its analogues were determined with radiolabeled

epothilone B. Epothilones are competitive inhibitors of paclitaxel binding, and the epothilones

retain activity against almost all known paclitaxel-resistant cell lines (Kowalski et al., 1997); the

exception is the 1A9/A8 line, which possess a mutation of Arg282->Gln in β-tubulin and is

resistant to both paclitaxel and epothilone B (Giannakakou et al., 2000). All of the agents tested

here were found to be competitive inhibitors of epothilone B's binding to tubulin polymer,

implying that dictyostatin and epothilone B share a common binding site on MTs.   As in the

saturation binding experiments with [^{14}C]epothilone B, significant ligand depletion was observed

in the competition experiments. For analysis of competition experiments with ligand depletion, it would be correct to assume that the inhibitor concentration would be depleted as well as substrate concentration. The modified Hanes analysis used by Edler et al. (Eq. 2) and employed here accounts for the free concentration of radiolabeled tracer and that of the free inhibitor (Edler et al., 2005).

In conclusion, a number of potent analogues of the microtubule stabilizer dictyostatin have been tested to determine the cellular responses they evoke, their effects on tubulin polymerization, and their ability to inhibit binding of $[^{14}C]$epothilone B to MTs. During this process, the saturation binding kinetics of epothilone B was characterized, and epothilone B demonstrated great affinity for the taxoid site. Dictyostatin and its analogues are all competitive inhibitors of $[^{14}C]$epothilone B binding as demonstrated by Hanes analysis. These experiments have further lead to the conclusion that dictyostatin, discodermolide, epothilone B, and paclitaxel have favorable interactions with Phe270 within the taxoid binding site on β-tubulin. A change to the configuration of the stereocenter at C6 or C7 of dictyostatin is well tolerated. From this work, it can be conjectured that for good efficacy against cancer cell lines, all future analogues of dictyostatin must retain the ability to interact with Phe270 on β-tubulin, and that this interaction is important to the efficacy of many other taxoid site-binding, MT-stabilizing compounds. The characterization of the 6-*epi*-dictyostatin analogue as a potent MT-stabilizing agent has motivated the gram scale synthesis for use in preclinical studies. Our QSAR analyses led to a number of equations that will be useful in guiding the production of and predicting the cellular activity of new, more potent dictyostatin analogues. The four descriptors employed in these equations are all variables that can be easily manipulated by a medicinal chemist.

Acknowledgements

References

Bollag DM, McQueney PA, Zhu J, Hensens O, Koupal L, Liesch J, Goetz M, Lazarides E and Woods CM (1995) Epothilones, a new class of microtubule-stabilizing agents with a taxol-like mechanism of action. *Cancer Res* 55:2325–2333.

Buey RM, Diaz F, Andreu JM, O'Brate A, Giannakakou P, Nicolau KC, Samai PK, Ritzen A, and Namato K (2004) Interaction of epothilone analogs with the paclitaxel binding site: Relationship between binding affinity, microtubule stabilization, and cytotoxicity. *Chem Biol* 11:225-236.

Carter CM, Leighton-Davies JR, and Charlton SJ (2007) Miniaturized receptor binding assays: Complications arising from ligand depletion. *J Biomol Screen* 12:255–266.

Edler MC, Buey RM, Gussio R, Marcus AI, Vanderwal CD, Sorensen EJ, Diaz JF, Giannakakou P, and Hamel E (2005) Cyclostreptin (FR182877), an antitumor tubulin-polymerizing agent deficient in enhancing tubulin assembly despite its high affinity for the taxoid site. *Biochemistry* 44:11525–11538.

Fukui Y, Brückner AM, Shin Y, Balachandran R, Day BW, and Curran DP (2006) Fluorous mixture synthesis of (–)-dictyostatin and three stereoisomers. *Org Lett* 8:301–304.

Gaitanos TN, Buey RM, Diaz JF, Northcote PT, Teesdale-Spittle P, Andreu JM and Miller JH

(2004) Peloruside A does not bind to the taxoid site on beta-tubulin and retains its activity in multidrug-resistant cell lines. *Cancer Res.* 64:5063-5067.

Giannakakou P, Sackett DL, Kang YK, Zhan Z, Buters JT, Fojo T, and Poruchynsky MS (1997) Paclitaxel-resistant human ovarian cancer cells have mutant beta-tubulins that exhibit impaired paclitaxel-driven polymerization. *J Biol Chem* 272:17118–17125.

Giannakakou P, Gussio R, Nogales E, Downing KH, Zaharevitz D, Bollbuck B, Poy G, Sackett D, Nicolaou KC, and Fojo T (2000) A common pharmacophore for epothilone and taxanes: Molecular basis for drug resistance conferred by tubulin mutations in human cancer cells. *Proc Natl Acad Sci USA* 97:2904–2909.

Giuliano KA, DeBiasio RL, Dunlay T, Gough A, Volosky JM, Zock J, Pavlakis GN, and Taylor DL (1997) High-content screening: a new aproach to easing key bottlenecks in the drug discovery process. *J Biomol Screen* 2:249–259.

Gunasekera SP, Gunasekera M, Longley RE, and Schulte GK (1990) Discodermolide: a new bioactive polyhydroxylated lactone from the marine sponge *Discodermia dissoluta.* *J Org Chem* 55:4912-4915.

Hamel E and Lin CM (1984) Separation of active tubulin and microtubule-associated proteins by ultracentrifugation and isolation of a component causing the formation of microtubule bundles. *Biochemistry* 23:4173–4184.

26

Hood KA, West LM, Rouwe B, Northcote, PT, Berridge, MV, Wakefield, SJ, and Miller, JH (2002) Peluroside A, a novel antimitotic agent with paclitaxel-like microtubule-stabilizing activity. *Cancer Res* 62:3356–3360.

Howard J and Hyman AA (2003) Dynamics and mechanics of the microtubule plus end. *Nature* 422:753–758.

Jordan MA and Wilson L (2004) Microtubules as a target for anticancer drugs. *Nat Rev* 4:253–265.

Jung WH, Harrison C, Shin Y, Fournier JH, Balachandran R, Raccor BS, Sikorski RP, Vogt A, Curran DP, and Day BW (2007) Total synthesis and biological evaluation of C16 analogs of (–)-dictyostatin. *J Med Chem* 50:2951–2966.

Kowalski RJ, Giannakakou P, and Hamel E (1997b) Activities of the microtubule-stabilizing agents epothilones A and B with purified tubulin and in cells resistant to paclitaxel (Taxol®). *J Biol Chem* 272:2534–2541.

Madiraju C, Edler MC, Hamel E, Raccor, BS, Balachandran R, Zhu G, Giuliano KA, Vogt A, Shin Y, Fournier JH, Fukui Y, Bruckner AM, Curran DP, and Day BW (2005) Tubulin assembly, taxoid site binding, and cellular effects of the microtubule-stablilizing agent dictyostatin. *Biochemistry* 44:15053–15063.

Minguez JM, Kim SY, Guillano KA, Balachandran R, Madiraju C, Day BW, and Curran DP

(2003) Synthesis and biological assessment of simplified analogues of the potent microtubule

stabilizer (+)-discodermolide. *Bioorg Med Chem* 11:3335–3357.

Mooberry SL, Tien G, Hernandez AH, Plubrukarn A and Davidson BS (1999) Laulimalide and

isolaulimalide, new paclitaxel-like microtubule-stabilizing agents. *Cancer Res* 59:653–660.

Morton MF, Harper EA, Tavares IA, and Shankley NP (2002) Pharmacological evidence for

putative CCK1 receptor heterogeneity in human colon smooth muscle. *Br J Pharmacol* 136:873–

882.

Motulsky H, and Christopoulos A (2003) *Fitting models to biological data using linear and

nonlinear regression. A practical guide to curve fitting.* GraphPad Software Inc., San Diego,

CA.

Padron JA, Carrasco R, and Pellon RF (2002) Molecular descriptor based on a molar refractivity

partition using Randic-type graph-theoretical invariant. *J Pharm Sci* 5:258–265.

Paterson I, Britton R, Delgado O and Wright AE (2004a) Stereochemical determination of

dictyostatin, a novel microtubule-stabilising macrolide from the marine sponge *Corallistidae* sp.

Chem Comm (Camb):632-633.

Paterson I, Britton R, Delgado O, Meyer A, and Poullennec KG (2004b) Total synthesis and configurational assignment of (–)-dictyostatin, a microtubule-stabilizing macrolide of marine sponge origin. *Angew Chem Int Ed Engl* 43:4629-4633.

Paterson I, and Gardner NM (2007a) Design, synthesis and biological evaluation of a macrocyclic discodermolide/dictyostatin hybrid. *Chem Commun (Camb)*:49-51.

Paterson I, Gardner NM, Poullennec KG, and Wright AE (2007b) Synthesis and biological evaluation of novel analogues of dictyostatin. *Bioorg Med Chem Lett* 17:2443–2447.

Pettit GR, Cichacz ZA, Gao F, Boyd MR, and Schmidt JM (1994) Isolation and structure of the cancer cell growth inhibitor dictyostatin 1. *J Chem Soc Chem Commun*: 1111-1112.

Pryor DE, O'Brate A, Bilcer G, Diaz JF, Wang Y, Wang Y, Kabaki M, Jung MK, Andreu JM, Ghosh AK, Giannakakou P and Hamel E (2002) The microtubule stabilizing agent laulimalide does not bind in the taxoid site, kills cells resistant to paclitaxel and epothilones, and may not require its epoxide moiety for activity. *Biochemistry* 41:9109–9115.

Reese M, Sanchez-Pedregal VM, Kubicek K, Meiler JM, Blommers MJJ, Griesinger C, and Carlomagno T (2007) Structural basis of the activity of the microtubule-stabilizing agent epothilone A studied by NMR spectroscopy in solution. *Angew Chem Int Ed Engl* 46:1864–1868.

Sanchez-Pedregal VM, Kubicek K, Meiler J, Lyothier I, Paterson I, and Carlomagno T (2006) The tubulin-bound conformation of discodermolide derived by NMR studies in solution supports a common pharmacophore model for epothilone and discodermolide. *Angew Chem Int Ed Engl* 45:7388–7394.

Sato B, Muramatsu H, Miyauchi M, Hori Y, Takase S, Hino M, Hashimoto S, and Terano H. (2000) A new antimitotic substance, FR182877. I. Taxonomy, fermentation, isolation, physico-chemical properties and biological activities. *J Antibiot (Tokyo)* 53:123-130.

Schiff PB, Fant J, and Horwitz SB (1979) Promotion of microtubule assembly in vitro by taxol. *Nature (London)* 277:665–667.

Shin Y, Fournier JH, Fukui Y, Bruckner AM and Curran DP (2004) Total synthesis of   (–)-dictyostatin: confirmation of relative and absolute configurations. *Angew Chem Int Ed Engl* 43:4634–4637.

Shin Y, Fournier JH, Balachandran R, Madiraju C, Raccor BS, Zhu G, Edler MC, Hamel E, Day BW, and Curran DP (2005) Synthesis and biological evaluation of (–)-16-normethyldictyostatin: A potent analogue of (–)-dictyostatin. *Org Lett* 7:2873–2876.

Shin Y, Fournier J-H, Bruckner A, Madiraju C, Balachandran R, Raccor BS, Edler MC, Hamel E, Sikorski RP, Vogt A, Day BW, and Curran DP (2007) Synthesis and biological evaluation of (–)-dictyostatin and stereoisomers. *Tetrahedron* 63:8537-8562.

Smith AB 3rd, LaMarche MJ, and Falcone-Hindley M (2001) Solution structure of (+)-discodermolide. *Org Lett* 3:695-698.

Smith AB 3rd, Freeze BS, LaMarche MJ, Hirose T, Brouard I, Xian M, Sundermann KF, Shaw SJ, Burlingame MA, Horwitz SB, and Myles DC (2005) Design, synthesis, and evaluation of analogues of (+)-14-normethyldiscodermolide. *Org Lett* 7:315–318.

Swillens S (1995) Interpretation of binding curves obtained with high receptor concentrations: Practical aid for computer analysis. *Mol Pharmacol* 47:1197–1203.

Verdier-Pinard P, Lai JY, Yoo HD, Yu J, Marquez B, Nagle DG, Nambu M, White JD, Falck JR, Gerwick WH, Day BW and Hamel E (1998) Structure-activity analysis of the interaction of curacin A, the potent colchicine site antimitotic agent, with tubulin and effects of analogs on the growth of MCF-7 breast cancer cells. *Mol Pharmacol* 53:62–76.

Xia S, Kenesky CS, Rucker PV, Smith AB, Orr GA, and Horwitz SB (2006) A photoaffinity analogue of discodermolide specifically labels a peptide in beta-tubulin. *Biochemistry* 45:11762–11775.

Footnotes

a) This work was supported by the NIH grant CA078039

b) Correspondence should be addressed to Dr. Billy W. Day. Mailing Address: 10017

Biomedical Sciences Tower 3, University of Pittsburgh, 3501 Fifth Avenue, Pittsburgh,

PA 15213. E-mail can be received at bday@pitt.edu

c) Department of Chemistry, University of Pittsburgh (B.S.R., Y.S., Y.F., W.-H.J., D.P.C.,

B.W.D.)

Department of Pharmacology, University of Pittsburgh (A.V., R.P.S.)

Drug Discovery Institute, University of Pittsburgh (A.V., K.M., B.W.D.)

Department of Pharmaceutical Sciences, University of Pittsburgh (C.M., R.B., B.W.D.)

*Primary laboratory of origin

Legends for figures

Figure 1. Structures of (–)-dictyostatin and (+)-discodermolide, their analogues used in these studies, and those of paclitaxel and epothilone B.

Figure 2. Immunofluorescence images of HeLa cells treated with dictyostatin and analogues. HeLa cells were treated with vehicle (DMSO) or with test agents for 20h followed by simultaneous immunostaining of α-tubulin (green), phosphohistone H3 (red), and nuclei (blue). **A**. Vehicle control. **B**. Dictyostatin (31 nM). **C**. 6-*epi*-Dictyostatin (7.8 nM). **D**. 7-*epi*-Dictyostatin (15.6 nM). **E**. 15Z,16-Normethyldictyostatin (19.5 nM). **F**. 16-Normethyldictyostatin (31 nM). Vehicle-treated cells have highly organized microtubules and a low percentage of mitotic cells. All compounds tested caused a heterogenous response of tubulin disorganization, increased numbers of phosphohistone H3 positive cells, enhanced chromatin condensation, and nuclear fragmentation. Images shown are representative from a single experiment that was repeated twice with each experiment yielding similar results.

Figure 3. Tubulin polymerization assay to determine effects of dictyostatin and its analogues on tubulin assembly. The reaction mixture contained 4% DMSO, 10 μM test agent, 10 μM bovine brain tubulin, and 0.75 M monosodium glutamate (MSG), pH 6.6. DMSO was the negative control and paclitaxel the positive control. All components except for test agents were cooled to 2.5 °C and test agents were added to cuvettes containing the reaction mixtures in a temperature-controlled spectrophotomer. One min after compound addition, the reaction mixtures were warmed to 30 °C. After 20 min at 30 °C, the reaction temperature was again dropped to 2.5 °C to determine the cold stability of polymer formed. (O), 4% DMSO. (□), (–)-Dictyostatin. (▼),

16-Normethyldictyostatin. (×), 15Z,16-Normethyldictyostatin. (♦), 6-*epi*-Dictyostatin. (✳),

7-*epi*-Dictyostatin. (△), Paclitaxel.

Figure 4. **Upper panel**: Saturation binding data for the binding of [^{14}C]epothilone B to

microtubules. Isolated tubulin was incubated with [^{14}C]epothilone B and the amount of protein-

bound radioactivity quantified as described in the Materials and Methods section. The x-axis

shows the total [^{14}C]epothilone B added and the y-axis the amount of ligand bound (■). Nine

concentrations in the range of 5 nM to 2 µM of radiolabeled epothilone B (■) were used to

determine the equilibrium binding constant (36.04 $\pm$ 1.58 nM). Nonspecific binding was

determined by competition with 8 µM discodermolide (▲). Each data point is a mean of three

independent experiments $\pm$ S.D. **Lower panel**: Hanes plot of the inhibition of binding of

[^{14}C]epothilone B to microtubules by 6-*epi*-dictyostatin. The y-axis is free substrate

concentration (µM)/fractional saturation (S/ν). All experiments yielded parallel lines with a

slope of ~1. The x-axis is free concentration of [^{14}C]epothilone B (µM). The fractional

saturation was calculated from the total amount of tracer added minus the free concentration of

tracer counted. Experiments were performed as described in the Materials and Methods section.

K_is were determined from the x-intercept, equal to $-(K_d(1+[I]/K_i)$. (■), No inhibitor µM. (▼),

(▲) and (♦), 6-*epi*-Dictyostatin at 1.6, 0.8 and 0.3 µM, respectively.

Figure 5. Graph of the –log (M) predicted versus –log (M) actual antiproliferative activities of

dictyostatin, discodermolide, the 12 analogues of dictyostatin, and 14-normethyldictyostatin in

1A9 human ovarian cancer cells. Predicted values were calculated from Eq. 1 (see text) in the

34

Cerius^2 suite of programs utilizing the genetic function approximation approach. The R^2 was for

this equation was 0.943.

Table 1. Potencies of dictyostatin and its analogues in HeLa cells using multiparameter fluorescence microscopy.

Compound	EC_{50} (nM)[a]	MDEC (nM)[a,b]		
	Cell Density	Nuclear Condensation	Mitotic Index[c]	Microtubule Mass
Paclitaxel	10.4 ± 1.9	3.9 ± 2.0	3.5 ± 1.2	5.2 ± 0.4
Dictyostatin	9.2 ± 6.6	3.9 ± 1.0	5.8 ± 1.5	5.4 ± 1.9
16-*epi*-Dictyostatin	1872 ± 449	1132 ± 66	1032 ± 173	1278 ± 181
16-*epi-seco*-Dictyostatin methyl ester	>5000	>5000	>5000	>5000
16-*epi*-Isodictyostatin	>5000	>5000	>5000	>5000
16-Normethyldictyostatin	34.7 ± 6.2	23.7 ± 8.8	24.1 ± 5.4	25.0 ± 9.0
7-*epi*-Dictyostatin	17.5 ± 1.9	7.7 ± 2.1	8.5 ± 3.9	8.0 ± 3.2
6-*epi*-Dictyostatin	8.9 ± 2.7	4.5 ± 1.9	3.8 ± 2.8	4.0 ± 0.9
2*E*,15*Z*,16-Normethyldictyostatin	896 ± 135	738 ± 214	520 ± 95	647 ± 106
15*Z*,16-Normethyldictyostatin	23.9 ± 15.5	12.6 ± 5.2	9.3 ± 0.2	11.7 ± 1.7
9-*epi*-15*Z*,16-Normethyldictyostatin	>5000	>5000	>5000	>5000
15*Z*,16-Normethylisodictyostatin	>5000	>5000	>5000	>5000

[a]Average of at least three independent experiments $\pm$ S.D. [b]Minimum detectable effective concentration. [c]Percentage of phosphohistone H3 positive cells.

Table 2. Equilibrium inhibition constants for dicytostatin and its analogues calculated from Hanes analysis of [^{14}C]epothilone B competition experiments. Concentrations used ranged from 0.25-12 μM for the inhibitors dictyostatin, 6-*epi*-dictyostatin and 7-*epi*-dictyostatin. For the less potent inhibitors, concentrations used ranged from 1-50 μM. [^{14}C]Epothilone B concentrations were 1, 2, 2.5 and 3 μM for all experiments. Free inhibitor concentration was calculated by subtracting the amount of tracer displaced by the inhibitor from the total amount of inhibitor added.

Compound	K_i (μM)
15Z,16-Normethyldictyostatin	4.47 ± 0.28
16-Normethyldictyostatin	4.55 ± 0.41
6-*epi*-Dictyostatin	0.48 ± 0.07
7-*epi*-Dictyostatin	0.93 ± 0.31
Dictyostatin	0.07 ± 0.02

Fig 1

	R^1	R^2	R^3	R^4
dictyostatin	*R*-Me	*S*-OH	*S*-OH	*S*-Me
16-normethyldictyostatin	*R*-Me	*S*-OH	*S*-OH	H
16-*epi*-dictyostatin	*R*-Me	*S*-OH	*S*-OH	*R*-Me
9-*epi*-16-normethyldictyostatin	*R*-Me	*S*-OH	*R*-OH	H
6-*epi*,7-*epi*-dictyostatin	*S*-Me	*R*-OH	*S*-OH	*S*-Me
6-*epi*-dictyostatin	*S*-Me	*S*-OH	*S*-OH	*S*-Me
7-*epi*-dictyostatin	*R*-Me	*R*-OH	*S*-OH	*S*-Me

	R
discodermolide	Me
14-normethyldiscodermolide	H

15Z,16-normethyldictyostatin
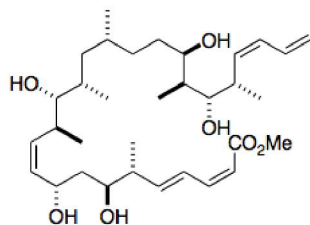
16-*epi*-*seco*-dictyostatin methyl ester
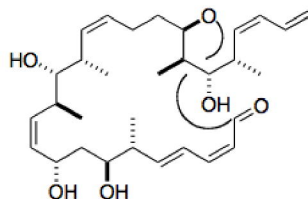
15Z,16-normethylisodictyostatin
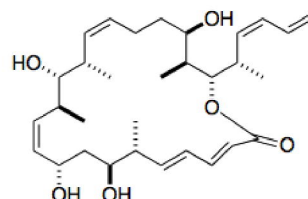
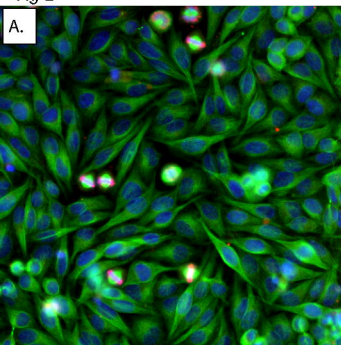**2E,15Z,16-normethyldictyostatin**
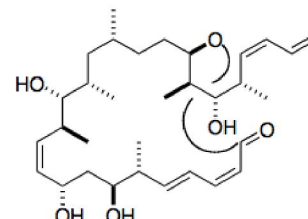
16-*epi*-isodictyostatin
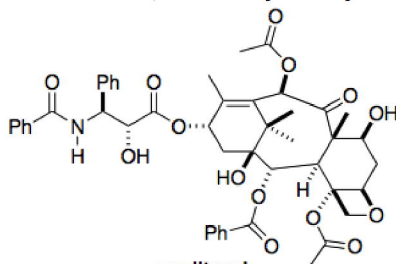
paclitaxel
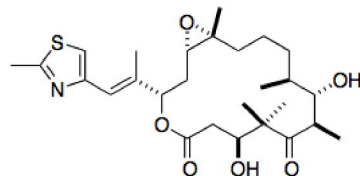
epothilone B

Fig 2

Fig 3

Fig 4

Fig 5